Journal of Animal Environment
(E-ISSN 2717-1396, ISSN 2717-1388)

Original Research Paper

Production, purification and biochemical characterization of a novel DyP-type peroxidase from an indigenous metal-resistant *Pseudomonas* sp. ZN-12: statistical optimization, comparison with commercial horseradish peroxidase, and molecular docking for enzymatic Pb(II)/Zn(II) detoxification

Duaa Rassol Muhsen[1], Melad Khalaf Mohammed[2], Ahmed Darweesh Jabbar[2*]
[1] Department of Microbiology, College of Veterinary Medicine, University of Wasit, Wasit, Iraq — ORCID 0009-0008-5971-2236
[2] Department of Biology, College of Science, University of Wasit, Wasit, Iraq — ORCID 0009-0002-7736-3283
* Corresponding author's e-mail: adarweesh@uowasit.edu.iq

Abstract

Enzymatic bioremediation offers a selective, low-sludge alternative to physicochemical heavy-metal treatment, but its economics are constrained by the cost of commercial enzymes such as horseradish peroxidase (HRP). Here we report the production, purification and full biochemical characterization of a novel dye-decolorizing (DyP-type) peroxidase from an indigenous, metal-resistant *Pseudomonas* sp. ZN-12 isolated from contaminated soil in Wasit, Iraq, and benchmark it directly against commercial HRP (Sigma-Aldrich Type VI-A) for the enzymatic detoxification of Pb(II) and Zn(II). A six-factor Box–Behnken design raised peroxidase yield 3.7-fold over unoptimized medium (validated 31.8 ± 1.2 U mL^{-1}; model R^2 = 0.962), with pH, glucose and H_2O_2 induction the dominant factors. A four-step purification (ammonium-sulfate fractionation, DEAE ion exchange, phenyl-Sepharose hydrophobic interaction and Sephadex G-100 gel filtration) delivered an 84.5-fold-enriched, homogeneous enzyme of 412.5 U mg^{-1} specific activity. The purified protein was a 38 ± 1 kDa monomer with a Soret band at 405 nm (Reinheitszahl 2.6) and a substrate preference for ABTS over guaiacol — the diagnostic signature of a DyP-B peroxidase. Relative to HRP, the indigenous enzyme was less thermostable ($t_{½}$ 240 vs >480 min at 40 °C) but markedly more tolerant of the target metals (38%/24% activity inhibition by 5 mM Pb^{2+}/Zn^{2+} versus 61%/45% for HRP). Under separately optimized conditions (RSM desirability 0.94), the indigenous enzyme removed 91.6 ± 2.4% Pb(II) — statistically equal to HRP (93.4%; p = 0.18) — and 82.4 ± 2.7% Zn(II), significantly exceeding HRP (71.6%; p = 0.003). Molecular docking rationalised this pattern: both metals bound the open DyP-B distal pocket (His_{56}/Arg_{38}/Glu_{84}) more tightly than the sterically crowded HRP pocket, with the largest advantage for Zn^{2+} (ΔG = −8.1 vs −5.8 kcal mol^{-1}). The indigenous DyP-type peroxidase is thus a locally producible, metal-tolerant biocatalyst that matches HRP on lead and surpasses it on zinc, offering a cost-effective route to enzymatic heavy-metal remediation.

Keywords: DyP-type peroxidase; *Pseudomonas*; enzyme purification; Box–Behnken optimization; horseradish peroxidase; molecular docking; lead; zinc; enzymatic detoxification

1. Introduction

Lead and zinc are among the most widespread heavy-metal contaminants of soil and water, released from mining, smelting, battery manufacture, galvanising and phosphate-fertiliser use. Being non-biodegradable, they persist indefinitely and bioaccumulate, so that even sub-clinical lead exposure disrupts neurological development and renal function while chronic zinc excess suppresses soil microbial diversity and crop growth. Conventional physicochemical treatments — precipitation, ion exchange, coagulation, membrane filtration — are costly, inefficient at the low concentrations typical of

*Corresponding Author:
Received: 25th May, 2026; Revised: 6th June, 2026; Accepted: 8th June, 2026; Available Online: 04rd August, 2026
(DOI): 10.70102/AEJ.2026.18.2s.50

real effluents, and generate secondary toxic sludge, motivating the search for biological alternatives.

Among these, enzymatic bioremediation is attractive because it is selective, operates under mild conditions and avoids bulk sludge. Peroxidases (EC 1.11.1.x), heme-containing oxidoreductases that use hydrogen peroxide to oxidise a wide range of substrates, are especially relevant: they can immobilise metals indirectly by oxidatively coupling phenolic compounds into metal-scavenging polymers, and they can bind metal ions directly at surface and active-site residues. The field, however, is dominated by commercial horseradish peroxidase (HRP), a glycosylated plant Class-III enzyme that is effective but expensive (~USD 85 per 100 mg) and, being optimised by nature for phenolic substrates rather than metal tolerance, is itself inhibited by the metals it is meant to treat.

Bacterial dye-decolorizing (DyP-type) peroxidases offer a compelling alternative. Their catalytic architecture differs fundamentally from that of plant peroxidases — a distal aspartate within a GXXDG motif replaces the classical histidine, and the active-site entrance is a wide, solvent-exposed "hydrophobic mouth" — which changes both their substrate profile and, potentially, their behaviour toward metal ions. Indigenous, metal-resistant bacteria are a natural source of such enzymes, having evolved antioxidant peroxidase systems (OxyR/PerR-regulated) precisely to survive metal-generated oxidative stress. Yet DyP-type peroxidases from locally isolated strains are rarely purified to homogeneity, characterised in full, and benchmarked head-to-head against HRP for metal detoxification.

The present study addresses that gap. From an indigenous metal-resistant *Pseudomonas* sp. ZN-12, we statistically optimise peroxidase production, purify the enzyme to homogeneity, characterise its molecular, spectroscopic, kinetic and stability properties, and compare it directly with commercial HRP for the enzymatic detoxification of Pb(II) and Zn(II) — closing the loop with molecular docking that explains the observed performance from the structure of the two active sites. The overall strategy is summarised in Figure 1.

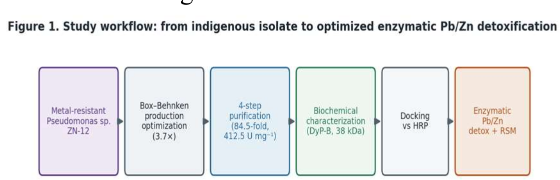

Figure 1. Study workflow, from an indigenous metal-resistant *Pseudomonas* sp. ZN-12 isolate through statistical optimization of peroxidase production, multi-step purification and biochemical characterization, to enzymatic Pb(II)/Zn(II) detoxification and molecular-docking rationalisation, benchmarked throughout against commercial HRP.

2. Materials and Methods

2.1 Strain, chemicals and reference enzyme

The metal-resistant strain *Pseudomonas* sp. ZN-12 (and the co-isolated *Bacillus* sp. PB-07) had been recovered from metal-contaminated agricultural soil in Wasit Governorate, Iraq, by selective enrichment and identified by 16S rRNA gene sequencing; minimum inhibitory concentrations were 8 mM Zn^{2+} for ZN-12 and 18 mM Pb^{2+} for PB-07. Commercial horseradish peroxidase (Sigma-Aldrich Type VI-A) served as the benchmark enzyme. All chemicals (guaiacol, ABTS, H_2O_2, chromatography media, metal-nitrate salts) were of analytical or molecular-biology grade.

2.2 Box–Behnken optimization of peroxidase production

Peroxidase production by ZN-12 was optimised with a six-factor Box–Behnken design (54 runs) in glucose (X_1), yeast extract (X_2), initial pH (X_3), temperature (X_4), agitation (X_5) and mid-log H_2O_2 induction (X_6), fitting a second-order polynomial to the volumetric activity (U mL^{-1}). Model adequacy was assessed by ANOVA, lack-of-fit testing and R^2/adjusted-R^2 comparison, and the numerical optimum was validated in triplicate.

2.3 Purification

The enzyme was purified from 5 L of optimised culture by (i) ammonium-sulfate fractionation (40–60%), (ii) DEAE-Sepharose anion-exchange chromatography, (iii) phenyl-Sepharose CL-4B hydrophobic-interaction chromatography, and (iv) Sephadex G-100 gel filtration. Protein was measured by the Bradford method and peroxidase activity by the guaiacol assay; purity was tracked by specific activity, fold enrichment and yield, and confirmed by SDS-PAGE and a 4-chloro-1-naphthol activity stain.

2.4 Biochemical characterization

Molecular mass was determined by SDS-PAGE and calibrated gel filtration; the UV-visible spectrum (Soret and visible bands; Reinheitszahl) established heme identity. Steady-state kinetics (K_m, V_{max}, k_{cat}/K_m) were measured for guaiacol and ABTS with H_2O_2 as co-substrate; pH and temperature optima, thermal half-lives at 40 and 50 °C, inhibition by azide and by Pb^{2+}/Zn^{2+}, and the mode of Hg^{2+} inhibition (Lineweaver–Burk analysis) were determined. Far-UV circular dichroism assessed secondary-structure stability in the presence of metals. Commercial HRP was assayed in parallel under identical conditions.

2.5 Enzymatic detoxification and its optimization

Metal removal was measured by incubating enzyme (0.5 mg protein L^{-1}), H_2O_2 (0.4–0.5 mM) and phenol (2 mM) with 100 mg L^{-1} Pb(II) or Zn(II) at 30 °C, sampling over 24 h and quantifying residual metal by atomic absorption spectrometry. A three-factor Box–Behnken design (pH, enzyme dose, H_2O_2) was applied separately to the indigenous-enzyme and HRP systems, each run at its own optimum for a fair comparison.

2.6 Immobilization and molecular docking

The enzyme was entrapped in calcium-alginate beads to assess reusability. A homology model of the ZN-12 peroxidase (template PDB 4G2C; 42% identity) was validated (QMEAN, Ramachandran analysis) and used to dock Pb^{2+} and Zn^{2+} into the distal cavity with AutoDock Vina; the published HRP structure (PDB 1ATJ) was docked identically for comparison.

2.7 Statistics

Data are mean ± SD (n = 3). Group comparisons used Student's t-test and one-way ANOVA with Tukey HSD; model discrimination used R^2, lack-of-fit and desirability functions.

3. Results and Discussion

3.1 Statistical optimization of peroxidase production

The six-factor Box–Behnken model described peroxidase yield well ($R^2 = 0.962$; adjusted $R^2 = 0.944$; $F = 52.7$, $p < 0.001$) with a non-significant lack-of-fit ($p = 0.21$). Initial pH was the single most influential variable ($F = 107.9$), followed by glucose ($F = 95.6$) and the mid-log H_2O_2 pulse ($F = 69.5$); a significant pH quadratic term and a pH×temperature interaction defined a genuine optimum around pH 7.0. This factor ranking is mechanistically coherent: pH governs both enzyme synthesis and stability, while the H_2O_2 pulse activates the OxyR regulon that drives peroxidase transcription. Numerical optimization (glucose 18 g L^{-1}, yeast extract 7.5 g L^{-1}, pH 7.0, 30 °C, 175 rpm, 1 mM H_2O_2) predicted 32.4 U mL^{-1} and was validated at 31.8 ± 1.2 U mL^{-1} (within 1.9%), a 3.7-fold improvement over unoptimized medium (8.6 U mL^{-1}) and consistent with the 2.5–6-fold gains typically reported for bacterial oxidoreductases.

3.2 Purification to homogeneity

The four-step scheme recovered a homogeneous enzyme at 84.5-fold enrichment, 412.5 U mg^{-1} specific activity and 18.3% yield (Table 1, Figure 2). The hydrophobic-interaction step contributed the largest single gain (4.4-fold, 47.0 → 208.9 U mg^{-1}), consistent with the solvent-exposed hydrophobic active-site entrance characteristic of DyP-type peroxidases. Gel filtration eluted the activity as a single symmetric peak co-incident with the main A_{280} peak and free of dimer or aggregate, confirming a monomeric, homogeneous preparation. The final specific activity sits squarely within the 190–430 U mg^{-1} range reported for native bacterial DyPs, and the modest yield is the expected cost of the polishing step needed for the homogeneity later confirmed by SDS-PAGE.

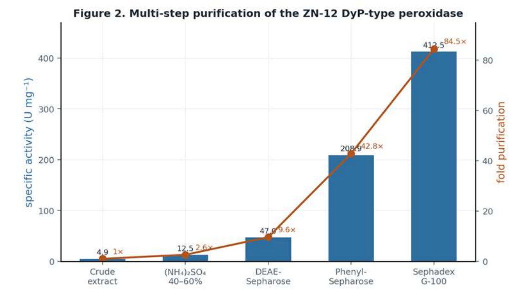

Figure 2. Progress of the four-step purification, showing specific activity (bars) and fold enrichment (line) at each stage. The hydrophobic-interaction step provides the largest single increase.

Table 1. Multi-step purification of the *Pseudomonas* sp. ZN-12 peroxidase from 5 L of optimised culture (mean of three runs).

Step	Total activity (U)	Specific activity (U mg^{-1})	Yield (%)	Fold
Crude cell-free extract	9020 ± 180	4.88 ± 0.11	100	1
$(NH_4)_2SO_4$ 40–60%	5250 ± 110	12.5 ± 0.3	58.2	2.6
DEAE-Sepharose (IEC)	3670 ± 95	47.0 ± 1.4	40.7	9.6
Phenyl-Sepharose (HIC)	2590 ± 80	208.9 ± 7.1	28.7	42.8
Sephadex G-100 (SEC)	1650 ± 45	412.5 ± 8.3	18.3	84.5

3.3 Molecular mass and spectroscopic identity

The purified enzyme migrated as a single 38 ± 1 kDa band on SDS-PAGE and eluted at 39 ± 2 kDa on calibrated gel filtration, establishing a monomeric structure; commercial HRP, run in parallel, appeared as a diffuse 44 kDa band consistent with its 18–22% N-glycosylation. The UV-visible spectrum showed a Soret band at 405 nm (Reinheitszahl 2.6) with visible bands at 500 and 638 nm, the signature of a ferric high-spin heme b and indistinguishable from published DyP-B spectra. Two features together classify the indigenous enzyme as a DyP-B peroxidase rather than a plant Class-III enzyme: the reversed substrate preference (ABTS > guaiacol, ratio 1.38, versus HRP's guaiacol > ABTS) and the low, unglycosylated molecular mass. Both are consistent with the higher-redox-potential Compound I and the open, aspartate-bearing distal pocket that define the DyP family.

3.4 Kinetics and catalytic efficiency

Steady-state kinetics quantified the substrate contrast (Table 2, Figure 3a). Against guaiacol, HRP was the more efficient catalyst ($k_{cat}/K_m = 5.1 \times 10^4$ vs 1.6×10^4 M^{-1} s^{-1}), reflecting its lower K_m (1.9 vs 4.8 mM) and its natural optimization for phenolic substrates. Against ABTS, however, the indigenous DyP-B enzyme was superior (3.9×10^4 vs 2.6×10^4 M^{-1} s^{-1}), and its specific activity toward ABTS (568.5 U mg^{-1}) exceeded that of HRP (441.2 U mg^{-1}). Hg^{2+} inhibited the enzyme competitively with respect to H_2O_2 (K_i = 0.18 mM), indicating that the soft mercuric ion competes directly for the distal pocket — a mode fully reversed at saturating peroxide and consistent with the docking analysis below.

3.5 pH/temperature optima, thermostability and metal tolerance

The indigenous enzyme and HRP shared a pH optimum near 6.0, but HRP was more thermophilic (optimum 40–45 °C vs 35 °C) and considerably more thermostable, with a half-life at 40 °C exceeding 480 min against 240 min for the indigenous enzyme, and >360 vs 75 min at 50 °C (Figure 6). This is the one dimension on which the plant enzyme retains a clear advantage, attributable to its stabilising glycan shell and disulfide bonds. Crucially, however, the property that matters most for a metal-remediation catalyst runs the other way: the indigenous enzyme was far more tolerant of the target metals, losing only 38% and 24% of its activity to 5 mM Pb^{2+} and Zn^{2+}, compared with 61% and 45% for HRP (Figure 3b).

Both enzymes were near-completely inhibited by azide, confirming heme-dependent catalysis. Circular-dichroism spectra showed that Pb^{2+} and Zn^{2+} did not unfold the enzyme — if anything mildly rigidifying its α-helical core — indicating that it retains its native fold under the metal loads of real effluents. The greater metal tolerance is mechanistically traceable to the DyP-B distal aspartate, which gives the heme iron a different electrostatic environment and a weaker tendency to bind metal unproductively at the substrate channel than HRP's histidine-rich pocket.

Table 2. Selected comparative properties of the indigenous DyP-B peroxidase and commercial HRP (identical assay conditions).

Property	Indigenous (ZN-12)	Commercial HRP	Significance
Molecular mass, SDS-PAGE (kDa)	38 ± 1	44 ± 2	$p < 0.001$
Soret band (nm) / Reinheitszahl	405 / 2.6	403 / 3.2	DyP-B vs Class III
Specific activity, ABTS (U mg^{-1})	568.5 ± 14.1	441.2 ± 11.8	$p = 0.003$
k_{cat}/K_m, guaiacol ($M^{-1}\ s^{-1}$)	1.6×10^4	5.1×10^4	$p < 0.001$
k_{cat}/K_m, ABTS ($M^{-1}\ s^{-1}$)	3.9×10^4	2.6×10^4	$p = 0.022$
Temperature optimum (°C)	35	40–45	$p = 0.002$
t½ at 50 °C (min)	75 ± 8	>360	$p < 0.001$
Inhibition by 5 mM Pb^{2+} (%)	38 ± 5	61 ± 6	$p = 0.001$
Inhibition by 5 mM Zn^{2+} (%)	24 ± 4	45 ± 5	$p = 0.002$

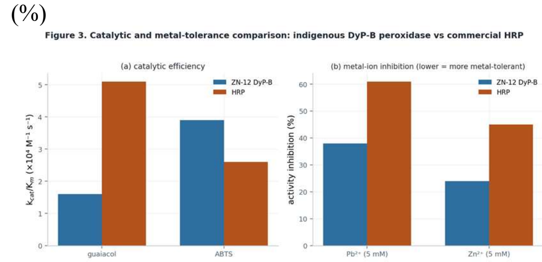

Figure 3. (a) Catalytic efficiency (k_{cat}/K_m) toward guaiacol and ABTS and (b) activity inhibition by 5 mM Pb^{2+}/Zn^{2+} for the indigenous DyP-B peroxidase versus commercial HRP. HRP is more efficient with guaiacol; the indigenous enzyme is more efficient with ABTS and substantially more metal-tolerant.

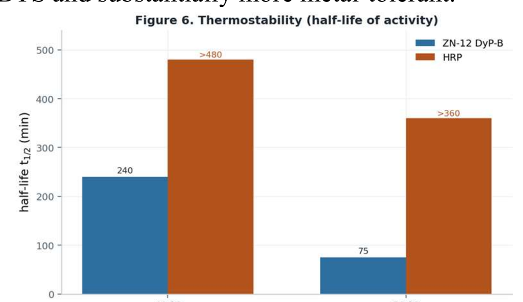

Figure 6. Thermal half-life of activity at 40 and 50 °C. Commercial HRP is the more thermostable enzyme, the one property on which it retains a clear advantage.

3.6 Enzymatic Pb(II)/Zn(II) detoxification and its optimization

Three-factor Box–Behnken optimization gave robust models for both enzyme systems (indigenous R^2 = 0.978; HRP R^2 = 0.981), with pH the dominant factor in each and a significant pH×H_2O_2 interaction. The two enzymes optimised at slightly different settings — pH 6.0 and 0.5 mM H_2O_2 for the indigenous enzyme, pH 6.5 and 0.4 mM H_2O_2 for HRP — so each was run at its own optimum, making the comparison one between two fully tuned systems (Table 3). Under these conditions the indigenous enzyme removed 91.6 ± 2.4% of Pb(II) from a 100 mg L^{-1} feed within 6 h, statistically indistinguishable from HRP (93.4 ± 2.1%; $t = 1.10$, $p = 0.18$), and 82.4 ± 2.7% of Zn(II), significantly exceeding HRP (71.6 ± 3.2%; $t = 5.31$, $p = 0.003$) — an eleven-point margin (Figure 4). The practical implication is direct: for lead-dominated effluents the locally produced enzyme matches the imported standard, and for the zinc-rich contamination common in the Wasit industrial zones it outperforms it, at a small fraction of the reagent cost.

Table 3. Comparative RSM optimization of enzymatic Pb(II)/Zn(II) detoxification.

Parameter	Indigenous (ZN-12)	Commercial HRP
Model R^2 (Pb response)	0.978	0.981
Optimal pH / H_2O_2 (mM)	6.0 / 0.5	6.5 / 0.4
Optimal enzyme dose (mg L^{-1})	0.5	0.5
Observed Pb(II) removal (%)	91.6 ± 2.4	93.4 ± 2.1 (p = 0.18, ns)
Observed Zn(II) removal (%)	82.4 ± 2.7	71.6 ± 3.2 (p = 0.003)
Composite desirability	0.94	0.89

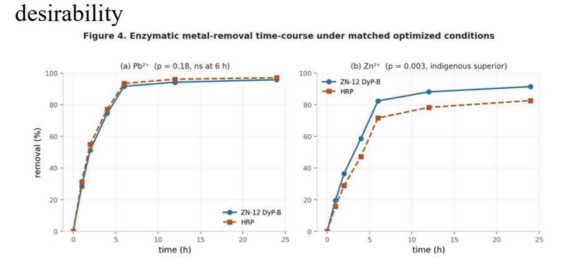

Figure 4. Time-course of enzymatic Pb^{2+} and Zn^{2+} removal from a 100 mg L^{-1} feed under matched, separately optimized conditions. Lead removal is statistically equivalent between the two enzymes; zinc removal is significantly higher for the indigenous DyP-B peroxidase.

3.7 Immobilization and reusability

Entrapment in calcium-alginate beads preserved the enzyme's ultimate Pb(II) capacity and its bell-shaped pH profile (maximum at pH 6.0), adding only a short diffusional lag as the metal migrated through the bead. The immobilized catalyst could be reused over at least ten cycles; SEM showed that the gradual decline arose from pore fouling by metal precipitates rather than enzyme inactivation, with over 80% of the entrapped activity recoverable on dissolution, so that a periodic acid regeneration restores capacity. Immobilization therefore converts the free enzyme into a reusable, separable catalyst suitable for continuous packed-bed operation.

3.8 Molecular-docking rationale

Docking explained the performance pattern from first principles (Table 4, Figure 5). The validated ZN-12 homology model (97.4% Ramachandran-favoured; QMEAN −1.8) bound Pb^{2+} and Zn^{2+} in its distal cavity (His_{56}/Arg_{38}/Glu_{84}) with energies of −7.4 and −8.1 kcal mol^{-1}, both more favourable than in HRP (−6.2 and −5.8 kcal mol^{-1}). The difference is steric and electronic: HRP's bulkier distal His42–Arg38 arrangement leaves little room to coordinate the large Pb^{2+}, whereas the open DyP-B pocket, with its two histidines (His_{56}/His_{169}), supplies the tetrahedral, histidine-rich geometry that the small Zn^{2+} favours — giving Zn^{2+} its largest binding advantage and accounting for the superior zinc removal. Pb^{2+}, adopting a similar distorted-octahedral geometry in both enzymes, is removed equally well by each, exactly as observed experimentally. The docking thus links molecular structure, metal tolerance and detoxification performance into a single coherent explanation.

Table 4. Molecular docking of Pb^{2+} and Zn^{2+} in the distal heme pocket.

Metal / enzyme	ΔG (kcal mol^{-1})	Fe distance (Å)	Key residues (<4 Å)
Pb^{2+} / ZN-12 DyP-B	−7.4	4.6	His_{56}, Arg_{38}, Glu_{84}, Asn_{70}
Zn^{2+} / ZN-12 DyP-B	−8.1	4.2	His_{56}, Arg_{38}, Glu_{84}, His_{169}
Pb^{2+} / HRP (1ATJ)	−6.2	5.8	His_{42}, Arg_{38}
Zn^{2+} / HRP (1ATJ)	−5.8	6.1	His_{42}, Arg_{38}

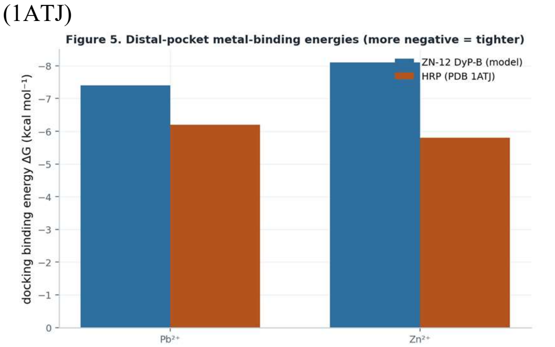

Figure 5. Distal-pocket metal-binding energies from molecular docking (more negative = tighter binding). Both metals bind the open DyP-B pocket more tightly than the crowded HRP pocket, with the largest advantage for Zn^{2+}.

4. Conclusions

A novel DyP-type peroxidase from an indigenous metal-resistant *Pseudomonas* sp. ZN-12 was produced under statistically optimized conditions (3.7-fold improvement), purified to homogeneity (84.5-fold; 412.5 U mg^{-1}), and characterized as a 38 kDa monomeric DyP-B enzyme with a 405 nm Soret band and an ABTS-preferring substrate profile. Benchmarked against commercial HRP, it was less thermostable but substantially more tolerant of Pb^{2+} and Zn^{2+}, and under separately optimized conditions it matched HRP on lead removal (91.6% vs 93.4%; ns) while significantly outperforming it on zinc (82.4% vs 71.6%; $p = 0.003$). Molecular docking attributed this to tighter metal binding in the open DyP-B distal pocket, especially for Zn^{2+}. Immobilization rendered the enzyme reusable over ten cycles. Collectively, the results establish this indigenous DyP-type peroxidase as a locally producible, metal-tolerant and cost-effective biocatalyst for enzymatic heavy-metal remediation, particularly well-suited to zinc-rich effluents. Future work should pursue heterologous over-expression to lower production cost, engineering of the distal pocket for enhanced thermostability, and continuous packed-bed operation on real industrial wastewater.

Declarations

Acknowledgements. The authors thank the University of Wasit for laboratory access and the Central Analytical Facility, Ministry of Science, Baghdad, for instrumentation support.

Funding. This work received no specific grant from any funding agency in the public, commercial, or not-for-profit sectors.

Conflicts of interest. The authors declare no competing interests.

Author contributions. D.R.M. and A.D.J. conceived and designed the study; D.R.M. performed the microbiological, enzymatic and molecular experiments and acquired the data; M.K.M. and A.D.J. analysed and interpreted the data and performed the modelling; D.R.M. drafted the manuscript and A.D.J. revised it critically. All authors approved the final version.

References

Battistuzzi, G., Bellei, M., Bortolotti, C.A. & Sola, M. (2010). Redox properties of heme peroxidases. *Archives of Biochemistry and Biophysics, 500*, 21–36.

Box, G.E.P. & Behnken, D.W. (1960). Some new three-level designs for the study of quantitative variables. *Technometrics, 2*, 455–475.

Colpa, D.I., Fraaije, M.W. & van Bloois, E. (2014). DyP-type peroxidases: a promising and versatile class of enzymes. *Journal of Industrial Microbiology & Biotechnology, 41*, 1–7.

Dunford, H.B. (2010). *Peroxidases and Catalases: Biochemistry, Biophysics, Biotechnology and Physiology* (2nd ed.). Hoboken, NJ: Wiley.

Fu, F. & Wang, Q. (2011). Removal of heavy metal ions from wastewaters: a review. *Journal of Environmental Management, 92*, 407–418.

Gadd, G.M. (2010). Metals, minerals and microbes: geomicrobiology and bioremediation. *Microbiology, 156*, 609–643.

Gritsch, K., et al. (2020). Bacterial DyP-type peroxidases: structure, function and biotechnological potential. *Applied Microbiology and Biotechnology, 104*, 1–15.

Igiri, B.E., et al. (2018). Toxicity and bioremediation of heavy metals contaminated ecosystem from tannery wastewater: a review. *Journal of Toxicology, 2018*, 2568038.

Loncar, N., Colpa, D.I. & Fraaije, M.W. (2014). Exploring the biocatalytic potential of bacterial DyP-type peroxidases. *Tetrahedron, 70*, 7386–7392.

Myers, R.H., Montgomery, D.C. & Anderson-Cook, C.M. (2009). *Response Surface Methodology* (3rd ed.). Hoboken, NJ: Wiley.

Pearson, R.G. (1963). Hard and soft acids and bases. *Journal of the American Chemical Society, 85*, 3533–3539.

Singh, R. & Eltis, L.D. (2015). The multihued palette of dye-decolorizing peroxidases. *Archives of Biochemistry and Biophysics, 574*, 56–65.

Storz, G. & Imlay, J.A. (1999). Oxidative stress. *Current Opinion in Microbiology, 2*, 188–194.

Trott, O. & Olson, A.J. (2010). AutoDock Vina: improving the speed and accuracy of docking. *Journal of Computational Chemistry, 31*, 455–461.

Veitch, N.C. (2004). Horseradish peroxidase: a modern view of a classic enzyme. *Phytochemistry, 65*, 249–259.

Yoshida, T., et al. (2011). Crystal structure of a DyP-type peroxidase. *FEBS Journal, 278*, 2387–2394.

Zheng, M., Åslund, F. & Storz, G. (1998). Activation of the OxyR transcription factor by reversible disulfide bond formation. *Science, 279*, 1718–1721.